Semicond. Sci. Technol. **22** (2007) 502–510 doi:10.1088/0268-1242/22/5/008

Effect of free-carrier absorption on performance of 808 nm AlGaAs-based high-power laser diodes

K A Bulashevich[1,2], V F Mymrin[2], S Yu Karpov[2,3], D M Demidov[4] and A L Ter-Martirosyan[4]

[1] Ioffe Physico-Technical Institute, Russian Academy of Sciences, St Petersburg 194021, Russia
[2] Soft-Impact Ltd, PO Box 83, St Petersburg 194156, Russia
[3] STR Inc, PO Box 70604, Richmond, VA 23255-0604, USA
[4] JSC 'ATC-Semiconductor Devices', PO Box 29, St Petersburg 194156, Russia

E-mail: karpov@semitech.us and ter@atcsd.ru

Received 4 October 2006, in final form 6 February 2007
Published 28 March 2007
Online at stacks.iop.org/SST/22/502

Abstract
We examine effects of free-carrier absorption produced by non-equilibrium electrons and holes injected in the waveguide on characteristics of high-power AlGaAs-based laser diodes emitting light at 808 nm. The carrier transport in the laser heterostructures is studied theoretically, using the drift-diffusion numerical approach. On the basis of simulations, a relation between the current density and non-equilibrium carrier concentrations in the waveguides is found. The internal optical losses of the waveguide modes and their effect on the differential quantum efficiency of the laser diodes are estimated from the computed carrier concentrations. Some approaches aimed at reducing the free-carrier absorption and, thus, improving the laser performance are discussed. The theoretical predictions are compared with available data to validate the theoretical model and justify the conclusions coming from the simulations.

1. Introduction

High-power laser diodes operating at 808 nm are widely employed for optical pumping of YAG:Nd^{3+} solid-state lasers [1]. This application requires primarily a high light output power and a small beam divergence combined with a high wall-plug efficiency of the laser diodes. In terms of laser parameters and characteristics, these requirements imply (i) a high catastrophic optical damage (COD) threshold of the output facet, (ii) a low series resistance of the diode, (iii) a high differential efficiency of coherent light emission and (iv) a narrow radiation far field.

To increase the COD threshold, three basic approaches are currently employed. The first one uses passivation of the laser output facet with a dielectric coating [2–5] to improve its chemical stability and reduce the non-radiative carrier recombination at the facet surface. The second approach utilizes an Al-free active region (see, for instance, [6–8]) that is found to be much more resistant to COD than a conventional AlGaAs one. The third approach invokes heterostructures with a low optical confinement factor, thus reducing the photon absorption and non-equilibrium carrier generation in the active layer near the output facet of the diode. A reduced optical confinement factor can be naturally obtained in the lasers with a wide waveguide [6, 7, 9, 10], providing at once a narrow emission far field [9, 10].

Reduction in the series resistance of the laser diodes can be achieved by optimization of the impurity doping and using graded-composition interfaces in the laser heterostructures instead of abrupt ones. Increasing of the donor and acceptor concentrations, primarily in the cladding layers, may lead, however, to higher internal optical losses due to free-carrier absorption and, eventually, to a lower differential efficiency of the lasers. Therefore, a careful optimization of doping is required to provide a lower series resistance without deterioration of other device characteristics.

Generally, to increase the differential quantum efficiency of a laser diode, one should reduce the internal optical

losses of the waveguide mode that first reaches the oscillation threshold. In AlGaAs-based devices, the internal losses are primarily controlled by free-carrier light absorption in the heterostructure. There are three main origins of the carrier absorption. The first one is the absorption in the cladding layers doped with donors or acceptors to provide the carrier access to the active region of the laser. The second origin is the light absorption in the active region where the concentration of the non-equilibrium carriers is extremely high. Despite a small active layer thickness, its contribution to the total absorption may be comparable with that of the claddings. The third origin is the light absorption in the nominally undoped waveguide where non-equilibrium electrons and holes are injected to. In wide waveguides, its contribution is especially important and may significantly affect the laser performance at high-current operation [11–13]. Therefore, optimization of high-power laser diodes should account for their operational conditions along with the heterostructure design itself.

To date, heterostructures with wide waveguides are conventionally employed for fabrication of high-power laser diodes [6, 9, 10, 14]. Nevertheless, pathways for their optimization are yet insufficiently understood. The reason for this is a limited number of studies dealing with specific mechanisms underlying the operation of the high-power lasers. In particular, comparably little attention was given to specific properties of AlGaAs alloys affecting the free-carrier absorption, role of graded-index (GRIN) materials in the carrier transport inside the heterostructure and effects of the non-equilibrium carrier injection in the waveguide on the laser characteristics, occurring at high operation currents through the diodes.

This paper reports on the combined theoretical and experimental study of 808 nm AlGaAs-based high-power laser diodes with the focus on free-carrier absorption effects that control the device performance. Mechanisms determining the optical losses in the heterostructures are examined in detail to identify the most important factors limiting the laser differential quantum efficiency. A number of approaches aimed at reducing the free-carrier absorption and, thereby, at improving the laser diode characteristics are discussed in terms of simulations. The experimental data are used to validate the theoretical model and justify the simulation-based conclusions.

The paper is organized as follows. Details of the laser diode heterostructure and fabrication procedure are described in section 2. The simulation approach and basic assumptions of the theoretical model are discussed in section 3. The results of the modelling analysis are presented in section 4, where a comparison of theoretical predictions with available observations is also done. The summary of the study and conclusions are given in section 5.

2. Fabrication of high-power laser diodes

The laser heterostructure was grown on a n^+-GaAs(0 0 1) substrate by sub-atmospheric metalorganic chemical vapour deposition (MOCVD), using TMGa, TMIn, TMAl, AsH_3, DMZn and Si_2H_6 as precursors. The structure consisted of a 0.3 μm n-GaAs buffer layer ($n = 2 \times 10^{18}$ cm^{-3}), a 1.5 μm n-$Al_{0.6}Ga_{0.4}As$ cladding layer ($n = 1 \times 10^{17}$ cm^{-3}), an undoped 0.15 μm GRIN AlGaAs waveguide layer with the AlAs molar fraction descending from 0.6 to 0.3, a 10 nm strained InGaAlAs active region providing the light emission at 808 nm, an undoped 0.15 μm graded-index AlGaAs waveguide layer with the AlAs molar fraction ascending from 0.3 to 0.6, a 1.5 μm p-$Al_{0.6}Ga_{0.4}As$ cladding layer ($p = 2 \times 10^{17}$ cm^{-3}) and a 0.2 μm p^+-GaAs contact layer ($p = 1 \times 10^{19}$ cm^{-3}). The background hole concentration in the nominally undoped GRIN waveguide layers was about 0.7–3.0 $\times$ 10^{16} cm^{-3}, according to capacitance–voltage measurements.

Broad-area laser diodes with the stripe width of 200 μm and the cavity length between 0.8 and 1.1 mm were fabricated from the above heterostructure. Ion etching was used to form a shallow mesa beyond the stripe followed by deposition of a 0.15 μm SiO_2 insulator film passivating the etched surface. Thinning of the GaAs substrate to 100 μm was applied before the ohmic contact formation. AuGe and AuZn alloys were chosen as the materials for n- and p-contact electrodes, respectively. High-reflective and low-reflective coatings were deposited on the output and back facets of the diodes, providing the fundamental mode reflectivities of 20% and 90%. To measure the laser CW characteristics, the samples were mounted on a polished Ni-covered cupper heat sink with the p-side down. The heat-sink temperature of 25 °C was controlled during the measurements.

3. Model and simulation approach

In order to analyse the operation of high-power lasers, we used the SiLENSe 1D-simulator initially developed for III-nitride wurtzite semiconductors [15] and adapted to cubic III–V compounds. The SiLENSe package implemented a drift-diffusion model of non-equilibrium carrier transport and accounted for the bimolecular radiative recombination of electrons and holes, their non-radiative Shockley–Read recombination, and the Auger recombination important at a high injection level. The simulator predicted the distributions of the electric potential, electron and hole concentrations, and recombination rates across the laser heterostructure for a certain forward bias applied. Then, such important parameters and characteristics were computed as the internal quantum efficiency (IQE) of spontaneous emission η_{int}, i.e. the ratio of the radiative recombination rate integrated over the heterostructure to the total recombination rate in the structure, the optical gain $g(\lambda)$ and its maximum value, and the current density j corresponding to the applied bias.

The SiLENSe simulator was supplemented with a special module computing the electromagnetic field in the waveguide. All the transverse waveguide modes were found from the solution of scalar wave equations derived from the Maxwell equations for a particular case of TE- or TM-polarization. The scalarization of the Maxwell equations was possible due to neglecting the edge effects related to the finite stripe width of the laser. Using the computed field distributions, the optical losses of every mode produced by the free-carrier absorption were calculated in a standard way (see, for instance, [16]). For this purpose, the local free-carrier absorption coefficients α_n and α_p were estimated from the computed electron n and hole

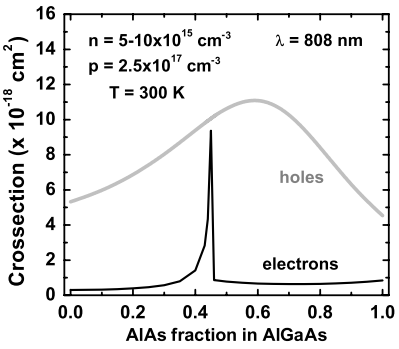

Figure 1. Free-carrier absorption cross-sections as a function of AlGaAs composition estimated from the data on electron and hole mobilities reported in [18, 19].

p concentrations by the expressions [17]

$$\alpha_n = \frac{q^3\lambda^2 n}{4\pi^2\mu_n m_n^2 N_r \epsilon_0 c^3}, \qquad \alpha_p = \frac{q^3\lambda^2 p}{4\pi^2\mu_p m_p^2 N_r \epsilon_0 c^3}, \quad (1)$$

where q is the electron charge, λ is the emission wavelength, c is the light velocity in vacuum, N_r is the refractive index of the semiconductor, ϵ_0 is the electric constant, μ_n and μ_p are the electron and hole mobilities, respectively, and m_n and m_p are the effective masses of electrons and holes. The optical losses were calculated separately for heavy and light holes, assuming the same mobility for each of them. The total hole absorption coefficient was found as the sum of the absorption coefficients related to the holes of both types. The contribution of split-off holes was ignored due to a negligible occupation of the split-off valence sub-band.

To illustrate the effect of the AlGaAs composition on the free-carrier absorption, we plotted in figure 1 the electron and hole absorption cross-sections, $\sigma_n = \alpha_n/n$ and $\sigma_p = \alpha_p/p$, calculated for $\lambda = 808$ nm, using equation (1) and the experimental data on electron and hole mobilities in AlGaAs reported in [18, 19]. Light holes are found to provide the major contribution to the hole cross-section because of a lower effective mass, and its dependence on the $Al_xGa_{1-x}As$ composition is related to the hole mobility variation primarily caused by alloy scattering [19]. A sharp peak in the electron cross-section at $0.4 < x < 0.5$ can be attributable to a dramatic electron mobility fall down observed in this composition range. The mobility reduction is apparently caused by strong intervalley electron scattering induced by the crossover of the Γ- and X-valleys in the conduction band [18]. It is worth noting that the electron cross-section σ_n plotted in figure 1 corresponds to undoped AlGaAs with the background electron concentration of 5–10 $\times$ 10^{15} cm^{-3}. If AlGaAs is doped with donors up to the concentration of $\sim 10^{17}$–10^{18} cm^{-3}, the cross-section $\sigma_n = \alpha_n/n$ may become several times larger because of a lower electron mobility controlled by the carrier scattering at ionized impurities. Even in the latter case, the hole cross-section is still considerably larger than the electron one. This fact is important to optimize the doping of a laser heterostructure.

The transverse mode first approaching the oscillation threshold, the threshold current density j_{th} and the output optical power P_{out} as a function of the current density were found from linearized rate equations relating the mean photon densities in the waveguide to the concentrations of non-equilibrium carriers. As a result, the following expression for the output power was derived (see, for instance, [20]):

$$P_{out} = \frac{\hbar\omega}{q}\eta_{st}(I - I_{th})\frac{\alpha_R}{\alpha_R + \alpha_i^{th}}F, \quad (2)$$

$$F = \frac{R_B^{1/2}(1 - R_O)}{\left(R_O^{1/2} + R_B^{1/2}\right)\left(1 - R_O^{1/2}R_B^{1/2}\right)}, \quad (3)$$

$$\alpha_R = \frac{1}{2L}\ln\frac{1}{R_O R_B}, \quad (4)$$

where $\hbar$ is the Plank constant, $\omega = 2\pi c/\lambda$ is the oscillation frequency, η_{st} is the quantum efficiency of stimulated emission, $I = jWL$ is the operation current, $I_{th} = j_{th}WL$ is the threshold current, W is the contact width, L is the cavity length, α_R is the coefficient of radiation losses, α_i^{th} is the internal absorption coefficient of the oscillating mode at the threshold current density, and R_O and R_B are the reflectivities of the output (with low-reflective coating) and back (with high-reflective coating) facets, respectively.

The quantum efficiency of stimulated emission η_{st} generally takes into account (i) the non-equilibrium carrier leakage from the active region and (ii) possible existence of ring modes in the laser cavity [16]. The losses of the former kind are directly considered within the electron/hole transport model, while the optical losses of the latter kind are ignored in our study. So, the deviation of η_{st} from unity is associated here with the carrier leakage.

The factor F in equation (3) accounts for the radiation losses through the back facet of the diode [20]; it is equal unity at $R_B = 1$. The differential quantum efficiency of a laser diode, $\eta_D = dP_{out}/dI$, can be readily obtained from equation (2).

The material properties of AlGaAs were largely borrowed from [16, 21]. To account for the crossover of Γ- and X-valleys in the Al_x Ga_{1-x} As conduction band, we separately consider the composition ranges $0 \leqslant x \leqslant 0.45$ and $0.45 \leqslant x \leqslant 1.0$, assigning them different material properties such as electron and hole effective masses, carrier mobilities, electron affinities and bandgaps as a function of the alloy composition. The Shockley–Read electron and hole lifetimes were estimated from the available data on the minority carrier diffusion lengths. To compute the Auger recombination rate, we used the Auger coefficient of 6 $\times$ 10^{-30} cm^6 s^{-1} obtained by averaging the experimental values reported in the literature for GaAs [22, 23].

4. Results

In this section, we will discuss the results of modelling the AlGaAs laser diode operation with the focus on mechanisms controlling the device performance at high current densities. The simulation results are compared with available observations in order to validate the theoretical approach applied.

4.1. Carrier injection and optical losses in high-power laser diodes

To investigate into mechanisms of non-equilibrium carrier injection, we consider at first the laser heterostructure

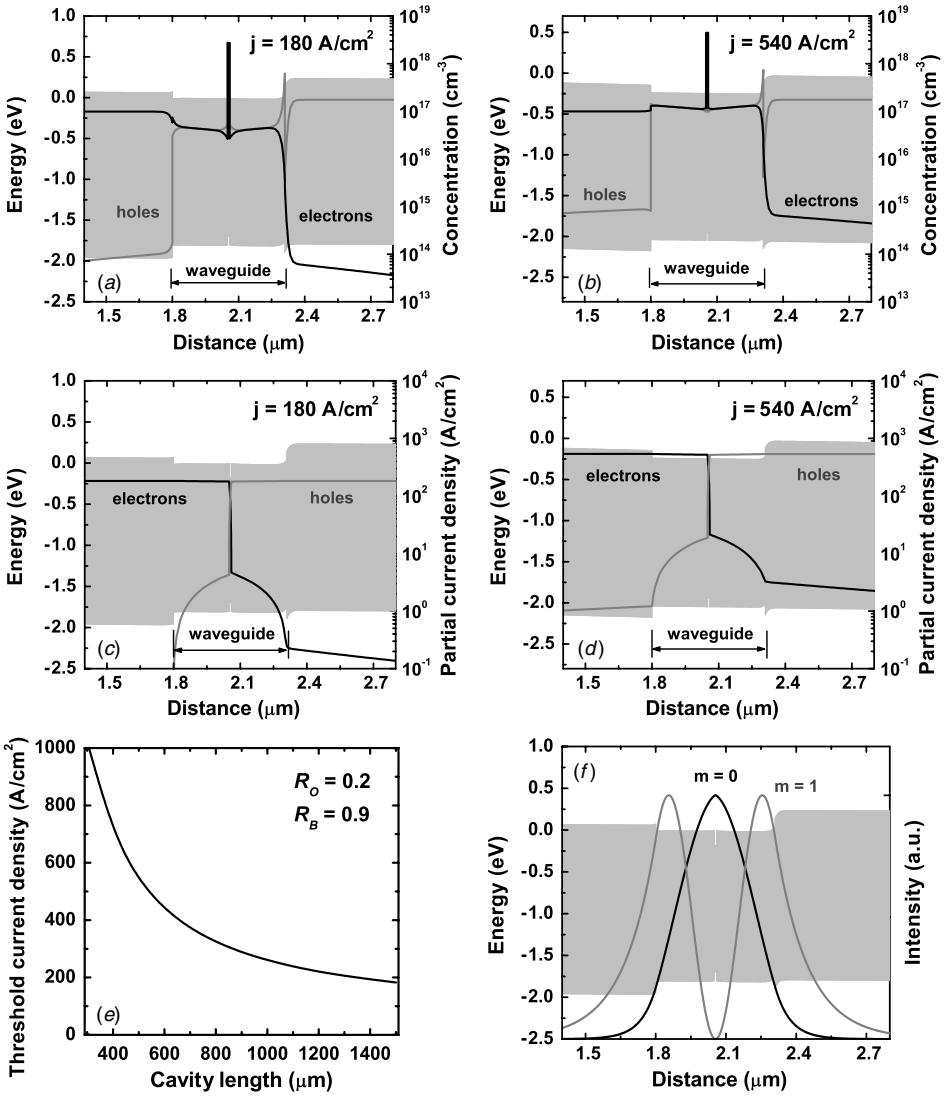

Figure 2. Band diagrams, carrier concentrations and partial electron and hole current densities in the laser structure with a 0.5 μm $Al_{0.3}Ga_{0.7}As$ waveguide corresponding to the threshold current density at the cavity lengths of 1500 μm (*a*), (*c*) and 500 μm (*b*), (*d*). Threshold current density of the laser diode as a function of the cavity length (*e*). Intensity distributions of the transverse modes in the laser heterostructure (*f*). The grey shadow in the plots indicates the bandgap.

consisting of a 1.5 μm *n*-$Al_{0.6}Ga_{0.4}As$ cladding layer ($n = 1 \times 10^{17}$ cm^{-3}), an undoped 0.5 μm $Al_{0.3}Ga_{0.7}As$ waveguide layer with a 10 nm $Al_{0.07}Ga_{0.93}As$ active layer placed in the centre of the waveguide, a 1.5 μm *p*-$Al_{0.6}Ga_{0.4}As$ cladding layer ($p = 2 \times 10^{17}$ cm^{-3}) and a 0.2 μm n^+-GaAs contact layer ($n = 1 \times 10^{19}$ cm^{-3}). The undoped waveguide is used to lower the free-carrier absorption in the structure.

Figures 2(*a*) and (*b*) compare the band diagrams and distributions of non-equilibrium carrier concentrations in the laser heterostructure, computed for the threshold current densities corresponding to the cavity lengths of 1500 and 500 μm. One can see that the conduction and valence bands in the structure are nearly flat with a slight slope in the waveguide layer, indicating the built-in electric field. In both cases, the electron and hole concentrations in the cladding layers are controlled by the respective donor and acceptor concentrations. In contrast, the carriers appear in the waveguide layers entirely due to injection. Our simulations demonstrate two specific features of the carrier injection. First, electrons and holes exist in the waveguide at nearly equal concentrations, providing electric neutrality of the waveguide layers. Second, the carrier concentration in the waveguide remarkably depends on the cavity length that determines the threshold current density (figure 2(*e*)). The concentration of electrons and holes is $\sim 4.5 \times 10^{16}$ cm^{-3} at $j_{\rm th} = 180$ A cm^{-2} and $\sim 1.2 \times 10^{17}$ cm^{-3} at $j_{\rm th} = 540$ A cm^2 (see figures 2(*a*), (*b*)). In the latter case, the concentration of the injected carriers even exceeds the electron concentration in the *n*-cladding layer. In order to understand this result, one can regard the drift component of the current density $j_{\rm drift}$ that is found to prevail over the diffusion component at $j > 160$–180 A cm^{-2}. Generally, $j_{\rm drift} \propto (\mu_n + \mu_p) nE$, where E is the built-in electric field in the waveguide. Under slight variation of E with the current density, which is confirmed by our simulation, the concentration of the injected carriers n is proportional to the current density. Therefore,

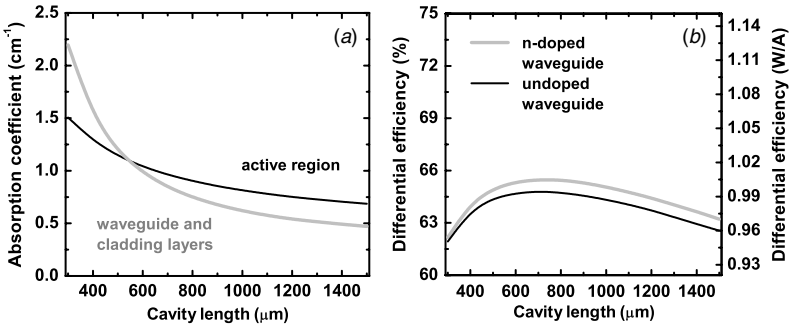

Figure 3. Optical losses of the fundamental mode related to free-carrier absorption in the active region and remainder of heterostructure, corresponding to the oscillation threshold (*a*). Differential quantum efficiency as a function of the cavity length for doped and undoped waveguide layers (*b*).

a smaller cavity length (a higher threshold current density) leads to a higher non-equilibrium carrier concentration in the waveguide. Since the electromagnetic field of a laser mode is largely concentrated in the waveguide layer (figure 2(*f*)), the increasing concentration of the injected electrons and holes results in a rise of optical losses in the waveguide and, eventually, in a lower differential quantum efficiency of the device.

Figures 2(*c*) and (*d*) show the distributions of partial electron and hole current densities in the laser heterostructure. One can see that even at the total current density of 540 A cm^{-2}, the carrier leakage does not exceed ∼4% . Only at the current density exceeding ∼1 kA cm^{-2} (the cavity length less than 300 μm), the leakage current becomes higher than ∼10% of the total current through the diode. This means that at the practically interesting cavity lengths ($L > 500$ μm), the non-equilibrium carrier leakage can be neglected.

Simulation predicts two transverse modes to exist in the laser structure (see figure 2(*d*)), having the optical confinement factors of $\Gamma_0 = 2.7\%$ and $\Gamma_1 = 0.001\%$. The very small value of Γ_1 results in the fact that only the fundamental ($m = 0$) mode is capable of reaching the oscillation threshold. Figure 3(*a*) shows the contribution of the active region and remainder of the laser heterostructure to the free-carrier absorption of the fundamental mode, as a function of the cavity length. One can see from the figure that the optical losses in the structure exceed those in the active region at $L < 540$ μm. This is due to the above-mentioned effect of the carrier injection in the waveguide, enhancing with the current density.

The dependence of the optical losses on the cavity length results also in a distinct maximum of the differential efficiency η_D at $L \approx 700$ μm (see figure 3(*b*)). As $\eta_D \propto \alpha_R / (\alpha_R + \alpha_i^{th})$ in accordance with equation (2), the decrease in the efficiency at $L > 700$ μm is related to lowering the coefficient of the radiation losses, α_R. At $L < 700$ μm the differential efficiency decreases because of a dramatic rise in α_i^{th} (see figure 3(*a*)).

The obtained results clearly demonstrate that the concentration of non-equilibrium carriers injected in the waveguide is an important factor limiting the performance of high-power laser diodes. Some ways to decrease the carrier concentration and, thus, to reduce the optical losses in the waveguide are discussed in the following sections of the paper.

4.2. Waveguide doping to reduce optical losses

It can be seen from figures 2(*a*) and (*b*) that concentrations of electrons and holes are nearly the same in every nominally undoped waveguide layer. As a result, both electrons and holes contribute to the free-carrier absorption in the waveguide in contrast to the *n*- and *p*-cladding layers where only electrons or holes, respectively, control the optical losses. On the other hand, holes provide the major contribution to the light absorption in the waveguide because of a remarkably larger cross-section σ_p (see figure 1). In this case, it becomes possible to reduce the total absorption by intentional *n*-doping of the waveguide layers. Indeed, the hole concentration in the waveguide is expected to be reduced under *n*-doping by the concentration of the ionized donors, which lowers the hole-mediated absorption. Since the electron cross-section σ_n is several times smaller than σ_p, the increase in the electron concentration does not lead in this case to a noticeable rise in the absorption coefficient.

To illustrate this concept, we consider the laser structure different from the structure specified in section 4.1 by intentional *n*-doping of the waveguide. The waveguide region between the *n*-cladding and active layer is assumed to be doped to the donor concentration of 1×10^{17} cm^{-3}, while the region between the active layer and the *p*-cladding to the donor concentration of 2×10^{17} cm^{-3}. The doping is found to slightly affect the threshold current density of the intentionally doped laser diode as compared to the undoped one.

Figure 4 plots the band diagrams and distributions of the carrier concentrations in the laser heterostructure with an *n*-doped waveguide computed for the threshold current densities at the cavity lengths of 1500 and 500 μm. One can see that the intentional doping provides a remarkable reduction in the concentration of holes injected in the waveguide. Despite an increase in the electron concentration, this leads to a reduced free-carrier absorption and, eventually, to a higher differential efficiency of the laser diode, as shown in figure 3(*b*). As in the case of the undoped waveguide heterostructure, the leakage current is found to be less than ∼4% of the total current through the diode for the cavity lengths $L > 500$ μm.

In the particular case considered above, the effect of the waveguide doping is not so strong. Nevertheless, it can be helpful for global optimization of high-power laser structures, especially of those having a relatively low optical confinement factor.

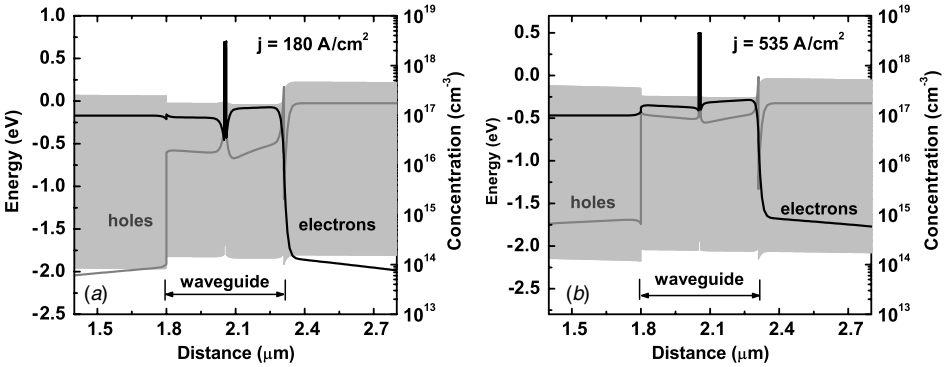

Figure 4. Band diagrams and carrier concentrations in the laser diode with an n-doped 0.5 μm $Al_{0.3}Ga_{0.7}As$ waveguide, corresponding to the threshold current densities at the cavity lengths of 1500 μm (a) and 500 μm (b). The grey shadow in the plots indicates the bandgap.

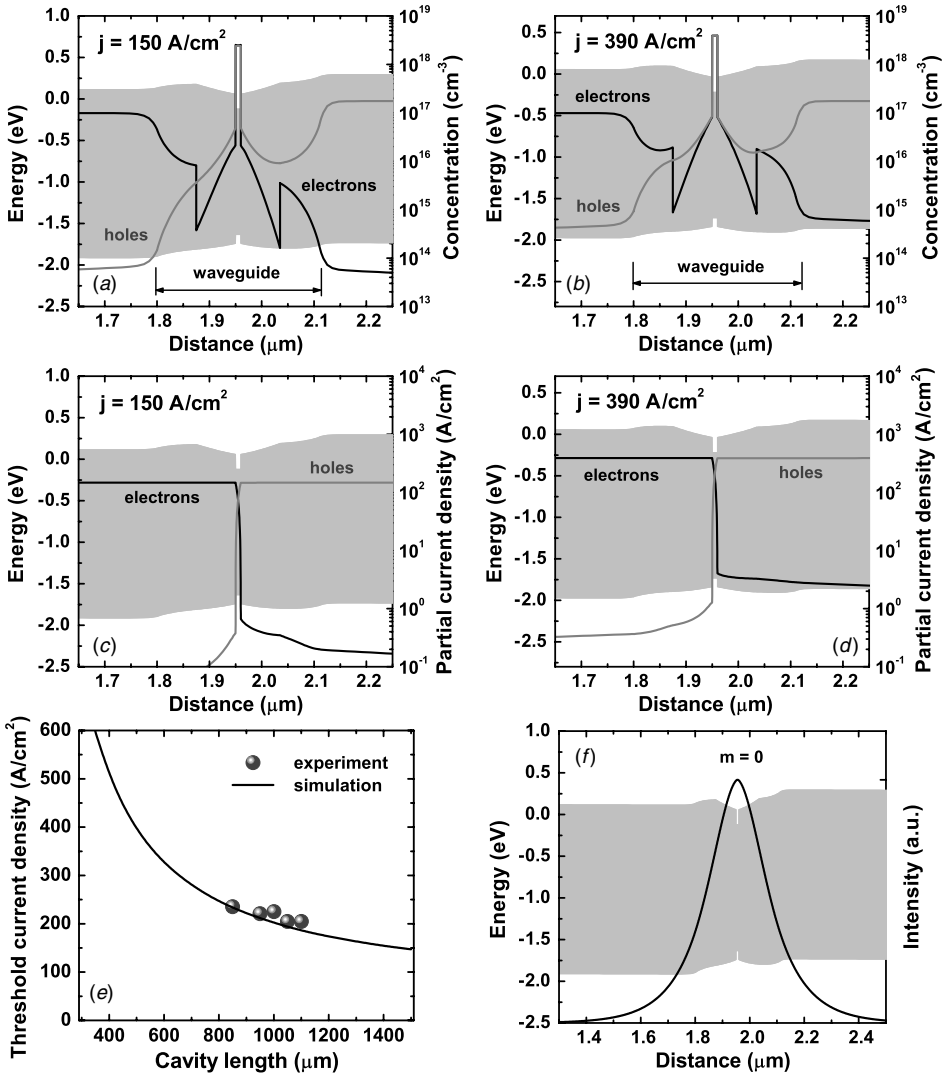

Figure 5. Band diagrams, carrier concentrations and partial electron/hole current densities in the laser diode with a GRIN waveguide corresponding to the threshold current densities at the cavity lengths of 1500 μm (a), (c) and 500 μm (b), (d). The threshold current density as a function of the cavity length (e). Intensity distribution of the fundamental mode in the laser heterostructure (f). The grey shadow in the plots indicates the bandgap. The balls are experimental data and lines are simulations.

4.3. Graded-index waveguides

One can realize from the relationship $j_{\text{drift}} \propto (\mu_n + \mu_p)nE$ between the drift component of the current density j_{drift} and the non-equilibrium electron or hole concentration in the waveguide n that a higher electric field E (a higher drift velocity of the carriers) favours the reduction of n and, hence, of internal optical losses. An effective way to enhance the carrier drift is the use of a GRIN waveguide, producing a built-in pulling

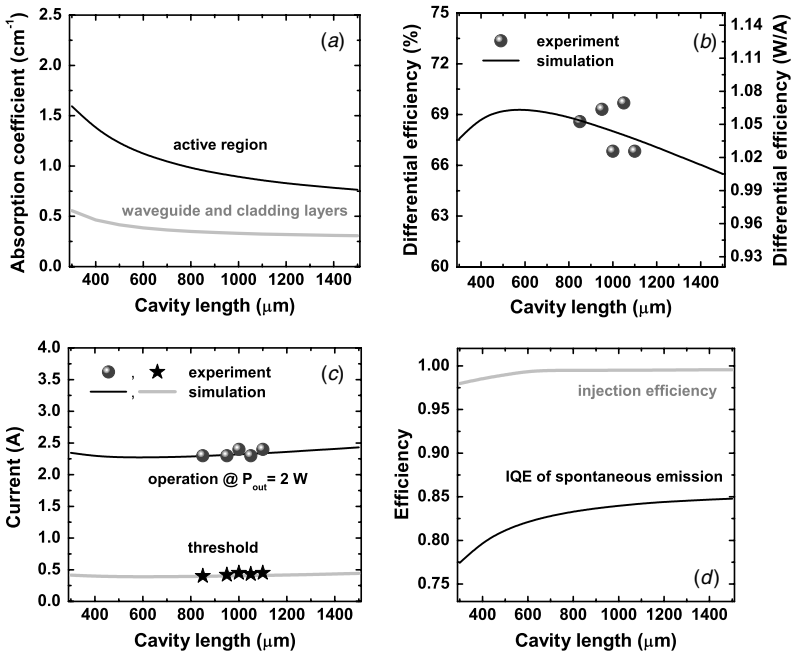

Figure 6. Optical losses of the fundamental mode at the oscillation threshold related to the free-carrier absorption in the active region and remainder of the structure (*a*). Differential quantum efficiency as a function of the cavity length (*b*). Predicted and measured threshold current and operation current corresponding to the output power of 2 W (*c*). Injection efficiency and internal quantum efficiency of spontaneous emission at the oscillation threshold as a function of the resonator cavity (*d*). All the plots correspond to the low- and high-reflective facet coatings providing the reflectivities of 20% and 90%, respectively.

field due to the bandgap variation in the graded-composition material. In order to examine this effect, we consider here the laser heterostructure specified in section 2.

Figures 5(*a*) and (*b*) present the band diagrams and distributions of electron and hole concentrations in the heterostructure computed for the threshold current densities related to the cavity lengths of 1500 and 500 μm. A specific feature of the band diagrams is a non-monotonic profile of the conduction band edge. This is due to the crossover of the Γ- and X-valleys resulting in an increasing conduction band offset between GaAs and AlGaAs with composition at $0 \leqslant x \leqslant 0.45$ and a decreasing offset at $0.45 \leqslant x \leqslant 1$. The crossover also leads in a drop/jump in the electron concentration at the positions corresponding to $x = 0.45$, the composition at which the crossover occurs. At this point, the density of states in the conduction band changes dramatically[5], and the electron concentration just follows these changes.

Simulation of the electromagnetic field in the laser structure predicts the only fundamental transverse mode to exist in the waveguide (figure 5(*d*)). Its optical confinement factor is found to be about 3.3%.

In contrast to the laser structure with the 0.5 μm $Al_{0.3}Ga_{0.7}As$ waveguide, the concentrations of electrons and holes in the structure with the GRIN waveguide is weakly interrelated with each other, so that no electric neutrality is produced in the waveguide layers. In addition, the concentration of the injected carrier in the GRIN waveguide is remarkably lower than in that having constant composition. The reason for such a behaviour is the built-in pulling field embedded in the graded-composition alloys, accelerating the carrier motion across the structure. As a result, the free-carrier losses beyond the active layer are considerably suppressed in the GRIN waveguide compared to those in the constant-composition one (see figure 6(*a*)). The reduced optical losses result in a higher differential efficiency of the laser with the GRIN waveguide.

To quantify the carrier leakage from the active region of the laser, we have computed the injection efficiency defined as the ratio of the total electron recombination current in the quantum well to the electron current in the *n*-cladding layer. The injection efficiency as a function of the cavity length is plotted in figure 6(*d*). One can see that the electron leakage is less than 2.5% even at the cavity as short as 300 μm. A similar estimate is also valid for holes. Figure 6(*d*) also shows the IQE of the spontaneous emission, η_{int}, computed for the threshold conditions. Actually, IQE accounts for the competition between the radiative and non-radiative recombination channels in the quantum well. As the carrier leakage from the active region is negligibly small, the dependence of IQE on the cavity length can be attributed to an increase in the non-radiative recombination rate largely because of the Auger recombination that becomes faster at a high current density (a low cavity length). The dominant contribution of the Auger recombination has been checked by 'switching off' this non-radiative recombination channel in some simulation cases.

Figures 5 and 6 compare the theoretical predictions for some of the laser characteristics with observations. A good agreement between the theory and experiment justifies the

[5] Actually, one can expect a steep monotonous variation of the electron concentration rather than a drop/jump, which is attributed to the step-like approximation of the AlGaAs material properties used in this study (see section 3).

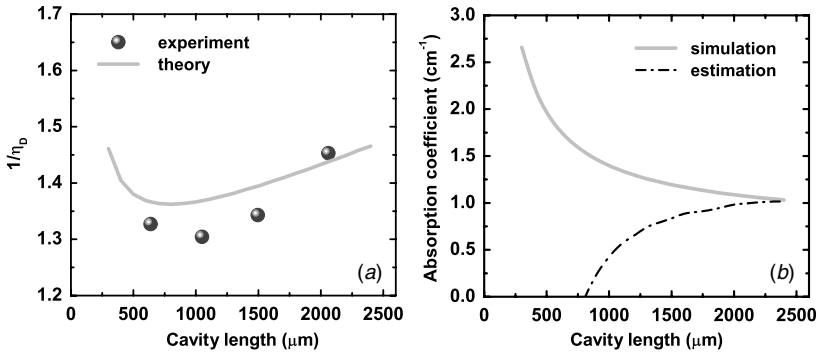

Figure 7. Inverse differential efficiency (*a*) and total free-carrier absorption coefficient (*b*) as a function of the cavity length in the laser diode with the GRIN waveguide and uncoated facets. The grey line is the simulation results, dot-dashed line is the estimate based on equation (6) and balls are experimental data.

applied approach and the main conclusions made on the basis of simulations.

4.4. On experimental estimation of optical losses

There is a well-known procedure for estimation of some important parameters of a laser heterostructure by plotting the total (per two facets) inverse differential efficiency of a diode with uncoated facets versus cavity length. For this purpose, a dimensionless efficiency is normally used, defined by the equation [16]

$$\eta_{\mathrm{D}}^{-1} = \eta_{\mathrm{st}}^{-1} \cdot \frac{\alpha_{\mathrm{R}} + \alpha_i^{\mathrm{th}}}{\alpha_{\mathrm{R}}}. \tag{5}$$

At $L \to 0$ the value of η_{D}^{-1} tends to η_{st}^{-1}. In turn, the slope of the $\eta_{\mathrm{D}}^{-1}(L)$ dependence provides the value of the absorption coefficient

$$\alpha_i^{\mathrm{th}} = \eta_{\mathrm{st}} \ln(1/R) \cdot \frac{\mathrm{d}\eta_{\mathrm{D}}^{-1}}{\mathrm{d}L}, \tag{6}$$

where R is the reflectivity of the uncoated facet nearly equal to 0.3.

The procedure fails, however, in the case of high-power lasers where the internal losses depend on the cavity length. First, there is no unambiguous way to extrapolate the dependence of $\eta_{\mathrm{D}}^{-1}(L)$ to zero value of L (figure 7(*a*)) because of its non-monotonic behaviour. Second, even if we accept that $\eta_{\mathrm{st}} = 1$, which is valid in the case of low carrier leakage from the active region, the absorption coefficient α_i^{th} determined from equation (6) becomes remarkably underestimated (see figure 7(*b*)), especially at the cavity lengths corresponding to the maximum of differential efficiency. Only at a very large L, at which the role of the carriers injected in the waveguide and active region is of less importance, the optical losses estimated by equation (6) become comparable with the actual values coming, for instance, from simulation (figure 7(*b*)).

As the above procedure is commonly used to estimate the optical losses and, thus, to assess the laser diode performance, the results obtained with this procedure may be misguiding. Much more reasonable seems the direct estimation of α_i^{th} from equation (5), assuming $\eta_{\mathrm{st}} = 1$ in a case of low carrier leakage from the active region or determining η_{st} from the data for very long cavities.

5. Conclusion

In this paper we have examined both theoretically and experimentally the effect of free-carrier absorption produced by electrons and holes injected in the waveguide on performance of high-power AlGaAs laser diodes. Using simulations, we have found that the concentration of the injected carriers remarkably depends on the cavity length (current density in the diode) and, in some cases, may exceed that in the cladding layers. In wide waveguides with a constant composition, the carrier transport occurs in such a way as to provide nearly equal concentrations of the injected electrons and holes that both contribute to the free-carrier absorption. Two approaches to lowering the injected carrier concentration are considered: (i) an intentional *n*-doping of a waveguide and (ii) the use of a graded-composition waveguide layer, where acceleration of the carrier motion across the waveguide is due to the built-in electric field. The latter way seems to be more promising than the former one. The dependence of the internal optical losses on the current density results in an optimum value of the cavity length that provides a maximum differential efficiency of the laser.

The theoretical predictions are in a good agreement with available observations that justify the main conclusions based on simulations.

References

[1] Steele R V 2004 Review and forecast of the laser market: II. Diode lasers *Laser Focus World* **40** 71–82
[2] Fukuda M 1991 *Reliability and Degradation of Semiconductor Lasers and LEDs* (Boston, MA: Artech House) chapters 4, 5 and 7
[3] Chand N, Hobson W S, de Jong J F, Parayanthal P and Chakrabarti V K 1996 ZnSe for mirror passivation of high-power GaAs based lasers *Electron. Lett.* **32** 1595–6
[4] Ueno Y 1998 Increased catastrophic-optical-damage output power for high-power semiconductor lasers coated with high-refractive-index films *Japan. J. Appl. Phys.* **37** L646–8
[5] Karsten L, Lindström V, Bluicht N P, Söderholm S H, Srinivasan A and Carlström C 2004 Method to obtain contamination free laser mirrors and passivation of these *US Patent* 681215282
[6] Wade J K, Mawst L J, Botez D and Morris J A 1998 8.8 W CW power from broad-waveguide Al-free active-region ($\lambda = 805$ nm) diode lasers *Electron. Lett.* **34** 1100–1

[7] Hayakawa T, Wada M, Yamanaka F, Asano H, Kuniyasu T, Ohgoh T and Fukunada T 1999 Effect of broad-waveguide structure in 0.8 μm high-power InGaAsP/InGaP/AlGaAs lasers *Appl. Phys. Lett.* **75** 1839–41
[8] Asonen H *et al* 1999 Al-free active area laser bar at 790–830 nm wavelengths *Proc. SPIE* **3628** 11–8
[9] Hülsewede R, Sebastian J, Wenzel H, Beister G, Knauer A and Erbert G 2001 Beam qualuity of high power 800 nm broad-area laser diodes with 1 and 2 μm large optical cavity structures *Opt. Commun.* **192** 69–75
[10] Knauer A, Erbert G, Staske R, Sumpf B, Wenzel H and Weyers M 2005 High-power 808 nm lasers with a superlarge optical cavity *Semicond. Sci. Technol.* **20** 621–4
[11] Garbuzov D Z, Ovchinnikov A V, Pikhtin N A, Sokolova Z N, Tarasov I S and Khalfin V B 1991 Experimental and theoretical investigations of singularities of the threshold and power characteristics of InGaAsP/InP separate-confinement double-heterostructure lasers ($\lambda = 1.3$ μm) *Sov. Phys. Semicond.* **25** 560
[12] Hirayama H, Yoshida J, Miyake Y and Asada M 1992 Estimation of carrier capture time of quantum-well lasers by spontaneous emission spectra *Appl. Phys. Lett.* **61** 2398–400
[13] Avrutin E A and Ryvkin B S 2005 Efficiency degradation due to carrier build-up in the broadened waveguides of high-power laser diodes: analytical theory and numerical validation *NUSOD'05. Proc. 5th Int. Conf. on Numerical Simulation of Optoelectronic Devices* pp 81–2
[14] Wang J, Smith B, Xie X, Wang X and Burnham G T 1999 High-efficiency diode lasers of high output power *Appl. Phys. Lett.* **74** 1525–7
[15] http://www.semitech.us/products/SiLENSe
[16] Casey H C Jr and Panish M B 1978 *Heterostructure Lasers* (New York: Academic) chapter 3
[17] Seeger K 1973 *Semiconductor Physics* (Berlin: Springer) chapter 11
[18] Saxena A K 1981 Electron mobility in $Ga_{1-x}Al_xAs$ alloys *Phys. Rev.* B **24** 3295–302
[19] Look D C, Lorance D K, Sizelove J R, Stutz C E, Evans K R and Whitson D W 1992 Alloy scattering in p-type $Al_xGa_{1x}As$ *J. Appl. Phys.* **71** 260–6
[20] Agrawal G P and Dutta N K 1986 *Long-Wavelength Semiconductor Lasers* (New York: Van Nostrand Reinhold) pp 60–1
[21] Adachi S 1985 GaAs, AlAs, and $Al_xGa_{1-x}As$: material parameters for use in research and device applications *J. Appl. Phys.* **58** R1–29
[22] Zory P S Jr 1993 *Quantum Well Lasers* (San Diego: Academic) pp 87, 163
[23] Cavalleri A *et al* 2001 Ultrafast x-ray measurement of laser heating in semiconductors: parameters determining the melting threshold *Phys. Rev.* B **63** 193306